JOURNAL OF THERMOPHYSICS AND HEAT TRANSFER
Vol. 6, No. 2, April–June 1992

Convective Thermal Ignition of an Individual Polymethylmethacrylate Particle

Gwo-Guang Wang* and Jing-Tang Yang†
National Tsing Hua University, Hsinchu, Taiwan 30043, Republic of China

The ignition process of a polymethylmethacrylate (PMMA) particle in a convective environment is studied theoretically and experimentally. The main parameters in this study are Reynolds number, gas temperature, initial particle size, and oxygen mass fraction. The effects of these parameters on the ignition delay time, first ignition position, ignition surface temperature, and ignition mechanism have been studied. The radiative effect is included in the theoretical model. For some test conditions, experiments were conducted to verify the model. The first ignition position and ignition delay time have been recorded experimentally. The theoretical results agree well with the experimental data qualitatively.

Nomenclature

A = pre-exponential factor
C_P = specific heat of gas mixture
D = mass diffusivity
d = fuel particle diameter
E = activation energy
F = view factor
k = thermal conductivity
L = heat of gasification
$\dot{m}''$ = pyrolysis rate
$\dot{m}'''$ = volumetric chemical reaction rate
n = stoichiometric ratio
Pr = Prandtl number
Q = heat of combustion
$q_{\text{cond},gs}$ = gas-solid conduction heat flux
$q_{\text{cond},s}$ = solid phase conduction heat flux
q_{ga} = gasification heat flux
$q_{\text{rad},was}$ = furnace wall-solid radiation heat flux
R_1 = fuel particle radius
R_2 = distance from symmetric axis to surface
Re = Reynolds number, $u_\infty R_1/\nu_\infty$
Re_d = Reynolds number, $u_\infty d/\nu_\infty$
r = radial coordinate
T = temperature
t = time
u = tangential velocity
v = radial velocity
x = peripheral coordinate
Y = mass fraction
y = normal coordinate

Greek Symbols

α = thermal diffusivity
ϵ = total emissivity
η = nondimensional position
μ = dynamic viscosity
ν = kinematic viscosity
ρ = density
σ = azimuthal angle, x/R_1
σ_{sb} = Stefan-Boltzmann constant, 1.356×10^{-12} cal/cm$^2 \cdot$ s $\cdot$ K^4

Subscripts

e = edge of boundary layer
F = fuel
g = gas
ga = gasification
i = solid phase initial value
O = oxygen
P = pyrolysis
R = reaction
s = solid phase
w = fuel surface
wa = furnace wall
∞ = freestream

Received Nov. 7, 1989; revision received March 26, 1990; accepted for publication March 27, 1990. Copyright © 1990 by the American Institute of Aeronautics and Astronautics, Inc. All rights reserved.

*Graduate Student, Department of Power Mechanical Engineering.
†Professor, Department of Power Mechanical Engineering.

Introduction

IGNITION has long been a subject of fundamental importance due to its close relation to the phenomena of flame spreading, flame stabilization, and flammability of fuels. Previous research laid great emphasis on radiative ignition for solid propellants,[1,2] or for polymer materials.[3] There is much research on steady-state convective burning for condensed fuel.[4,5] Studies concerning the transient ignition of solid fuel or condensed fuel are rare. Only a few theoretical[6-9] and experimental[10,11] studies have been done.

There exist three modes of ignition for solid fuels: gas phase ignition, solid phase ignition, and heterogeneous ignition, with the gas phase ignition being the main mode for most solid fuel ignition under convective heating. Amos and Fernandez-Pello[8] studied the ignition and flame development on a vaporizing combustible surface due to the absorption of radiation energy by the gas phase fuel vapor. The study treated the solid phase as steady-state and assumed the solid phase to be at the vaporization temperature.

Niioka et al.[10,11] studied experimentally the ignition of polymers and propellants under a convective hot flow. The results revealed the existence of a critical velocity, where the ignition delay is a minimum. Niioka's theoretical work[12] also proposed a dimensionless number of the stretch rate of flow which could reasonably interpret the phenomena. However, they assumed that ignition always initiated at the stagnation point. In addition, their results were limited to the high velocity region due to experimental apparatus limitations.

The problem of ignition position has been studied theoretically by Rangel et al.[13] for premixed combustible flows over a catalytic or noncatalytic surface. Kashiwagi and Summerfield[14] found that the first ignition position of the solid polymeric fuel plate could be shifted when the oxygen concentration of the flowfield was changed. They also pointed out that

the nonsimilar calculation was better than local similarity calculation for analyzing the ignition behavior of the solid fuels. Yang et al.[6] studied the ignition process of polymer ignition under convective environment and discussed the effect of oxygen mass fraction on the ignition position.

Since the completed governing equations of ignition of a solid fuel particle are too complicated to solve, in this paper a simplified theoretical model based on the nonsimilar boundary-layer theory is developed for the preliminary study of the ignition delay time, ignition position, and surface temperature at ignition of a single polymethylmethacrylate (PMMA) particle in a convective environment. Analyzed were the effects of the Reynolds number, oxygen mass fraction, gas temperature, and initial particle size on the ignition delay time, ignition surface temperature, and first ignition position. The model deals with only the preignition stage, and the phenomena of flame development and spreading are not included. The ignition process of PMMA particles in a high temperature furnace was observed experimentally using a video camera. The ignition delay time was recorded and compared with the theoretical predictions to verify the validity of the model.

Theoretical Model

The physical problem of the theoretical model is shown in Fig. 1 schematically. Hot air flows over a spherical PMMA particle and forms the momentum and the thermal boundary layers. The PMMA particle is heated by the hot convective air as well as the radiative heat emitted from the furnace wall and then pyrolyzes. The pyrolyzed vapor diffuses into the boundary layer and reacts with the hot oxidizing gas. The heat released from the reaction feeds back to the particle surface and enhances both the pyrolysis rate and the chemical reaction rate. When the thermal runaway occurs at a certain position, ignition takes place, and the flame starts to spread over the whole particle surface.

Since the ignition process is a complicated phenomenon, and the mathematical model is highly nonlinear and extremely complex, the following assumptions are made for simplicity:

1) The characteristic time for the gaseous phase process is much shorter than that of the solid phase, so the boundary-layer equations for the gas phase are regarded as quasisteady.

2) The boundary layer is laminar before the separation point.

3) The pyrolysis rate $\dot{m}_P''$ of the fuel is expressed by an Arrhenius pyrolysis law and depends only upon the surface temperature,

$$\dot{m}_P'' = \rho_s A_P \exp(-E_P/RT_W) \tag{1}$$

4) The volumetric pyrolysis inside the solid fuel is negligible, and the specific heat, the conductivity, and the density are constants.

5) The chemical reaction is described by a one-step, second-order Arrhenius kinetics. The volumetric chemical reaction rate $\dot{m}_R'''$ is expressed as

$$\dot{m}_R''' = A_R \rho^2 Y_O Y_F \exp(-E_R/RT) \tag{2}$$

6) The gas mixture obeys the ideal gas law.

7) The gases are transparent with respect to radiation, and only the radiative heat transfer between the furnace wall and the particle surface is considered.

The origin of the coordinate system of the gas phase equations is at the front stagnation point of the particle. The x axis is along the fuel surface, and the y axis is perpendicular to the x axis. The origin of the solid phase equation is at the center of the fuel, as depicted in Fig. 1.

Gas Phase Governing Equations

Continuity:

$$\frac{\partial(R_2\rho u)}{\partial x} + \frac{\partial(R_2\rho v)}{\partial y} = 0 \tag{3}$$

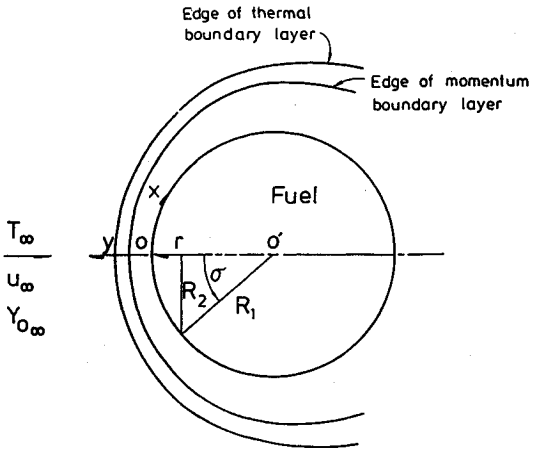

Fig. 1 Physical configuration of the model.

Momentum:

$$\rho u\frac{\partial u}{\partial x} + \rho v\frac{\partial u}{\partial y} = \rho_e u_e\frac{du_e}{dx} + \frac{\partial}{\partial y}\left(\mu\frac{\partial u}{\partial y}\right) \tag{4}$$

where u_e is the velocity of air external to the momentum boundary layer and can be calculated from the potential flow theory as

$$u_e = \frac{3}{2}u_\infty \sin\frac{x}{R_1} \tag{5}$$

Energy:

$$\rho u C_P\frac{\partial T}{\partial x} + \rho v C_P\frac{\partial T}{\partial y} = \frac{\partial}{\partial y}\left(k\frac{\partial T}{\partial y}\right) + Q\rho^2 Y_O Y_F A_R \exp(-E_R/RT) \tag{6}$$

Oxidizer species:

$$\rho u\frac{\partial Y_O}{\partial x} + \rho v\frac{\partial Y_O}{\partial y} = \frac{\partial}{\partial y}\left(\rho D\frac{\partial Y_O}{\partial y}\right) - n\rho^2 Y_O Y_F A_R \exp(-E_R/RT) \tag{7}$$

Fuel species:

$$\rho u\frac{\partial Y_F}{\partial x} + \rho v\frac{\partial Y_F}{\partial y} = \frac{\partial}{\partial y}\left(\rho D\frac{\partial Y_F}{\partial y}\right) - \rho^2 Y_O Y_F A_R \exp(-E_R/RT) \tag{8}$$

Equation of state:

$$\rho T = \rho_\infty T_\infty \tag{9}$$

where it is assumed that the pressure change is small across the y direction.

The boundary conditions for the above governing equations are as follows.

At $x = 0$

$$u = 0 \tag{10a}$$

$$\frac{\partial T}{\partial x} = 0 \tag{10b}$$

$$\frac{\partial Y_O}{\partial x} = 0 \tag{10c}$$

$$\frac{\partial Y_F}{\partial x} = 0 \tag{10d}$$

At $y = 0$

$$u = 0 \tag{11a}$$

$$v = v_w = \frac{\rho_s v_s}{\rho_w} = \frac{\rho_s}{\rho_w} A_P \exp(-E_P/RT_w) \tag{11b}$$

$$T_s = T_w \tag{11c}$$

$$q = q_{\text{rad},was} + q_{\text{cond},gs} = q_{\text{ga}} + q_{\text{cond},s} \tag{11d}$$

$$-\rho_w D_w \frac{\partial Y_O}{\partial y}\bigg|_w + \rho_w v_w Y_{O_w} = 0 \tag{11e}$$

$$-\rho_w D_w \frac{\partial Y_F}{\partial y}\bigg|_w + \rho_w v_w Y_{F_w} = \rho_s v_s \tag{11f}$$

where

$$q_{\text{rad},was} = \sigma_{sb} F_{w-wa} \epsilon_w \epsilon_{wa} (T_{wa}^4 - T_w^4) + \sigma_{sb} \epsilon_w \sum_{i=1}^{2} \epsilon_i F_{w-i} (T_i^4 - T_w^4) \tag{12a}$$

$$q_{\text{cond},gs} = k_w \frac{\partial T}{\partial y}\bigg|_w \tag{12b}$$

$$q_{\text{ga}} = \rho_s v_s L \tag{12c}$$

$$q_{\text{cond},s} = k_s \frac{\partial T_s}{\partial r}\bigg|_{R_1} \tag{12d}$$

At $y = \infty$

$$u = \frac{3}{2} u_\infty \sin \frac{x}{R_1} \tag{13a}$$

$$T = T_\infty \tag{13b}$$

$$Y_O = Y_{O_\infty} \tag{13c}$$

$$Y_F = 0 \tag{13d}$$

Solid Phase Equation

Energy:

$$\frac{1}{r}\frac{\partial^2}{\partial r^2}(rT_s) = \frac{1}{\alpha_s}\frac{\partial T_s}{\partial t} \tag{14}$$

The initial condition for the solid phase energy equation is, when $t = 0$,

$$T_s = T_i \tag{15}$$

The boundary conditions for the solid phase energy equation are, at $r = 0$,

$$\frac{\partial T_s}{\partial r} = 0 \tag{16a}$$

At $r = R_1$

$$T = T_w \tag{16b}$$

The following dimensionless variables are introduced

$$\sigma = x/R_1 \tag{17}$$

$$\eta = \left(\frac{3}{2} Re\right)^{1/2} \frac{1}{R_1} \int_0^y \frac{\rho}{\rho_\infty} dy \tag{18}$$

$$R_2 = R_1 \sin \sigma \tag{19}$$

where the Howarth transformation is used to transform the compressible equation into an incompressible form. In addition, a stream function ψ is defined as

$$R_2 \rho u = \mu_\infty \frac{\partial(\psi R_2)}{\partial y} \tag{20}$$

$$R_2 \rho v = -\mu_\infty \frac{\partial(\psi R_2)}{\partial x} \tag{21}$$

With the defined variables and the assumptions, Eq. (4) and Eqs. (6–8) can be transformed into

$$\frac{\partial\psi}{\partial\eta}\frac{\partial^2\psi}{\partial\sigma\partial\eta} - \left(\frac{\partial\psi}{\partial\sigma} + \psi \cot\sigma\right)\frac{\partial^2\psi}{\partial\eta^2} = \left(\frac{3}{2} Re\right)\frac{\rho_\infty}{\rho} \sin\sigma\cos\sigma + \left(\frac{3}{2} Re\right)^{1/2}\frac{\partial^3\psi}{\partial\eta^3} \tag{22}$$

$$\frac{\partial\psi}{\partial\eta}\frac{\partial T}{\partial\sigma} - \left(\frac{\partial\psi}{\partial\sigma} + \psi \cot\sigma\right)\frac{\partial T}{\partial\eta} = \left(\frac{3}{2} Re\right)^{-1/2} Pr^{-1}\frac{\partial^2 T}{\partial\eta^2} + \left(\frac{3}{2} Re\right)^{-1/2}\frac{\rho_\infty^2 R_1^2 Q}{\mu_\infty C_P}\frac{\rho}{\rho_\infty} Y_O Y_F A_R \exp(-E_R/RT) \tag{23}$$

$$\frac{\partial\psi}{\partial\eta}\frac{\partial Y_O}{\partial\sigma} - \left(\frac{\partial\psi}{\partial\sigma} + \psi \cot\sigma\right)\frac{\partial Y_O}{\partial\eta} = \left(\frac{3}{2} Re\right)^{1/2} Pr^{-1}\frac{\partial^2 Y_O}{\partial\eta^2} - \left(\frac{3}{2} Re\right)^{-1/2}\frac{\rho_\infty^2 R_1^2 n}{\mu_\infty}\frac{\rho}{\rho_\infty} Y_O Y_F A_R \exp(-E_R/RT) \tag{24}$$

$$\frac{\partial\psi}{\partial\eta}\frac{\partial Y_F}{\partial\sigma} - \left(\frac{\partial\psi}{\partial\sigma} + \psi \cot\sigma\right)\frac{\partial Y_F}{\partial\eta} = \left(\frac{3}{2} Re\right)^{1/2} Pr^{-1}\frac{\partial^2 Y_F}{\partial\eta^2} - \left(\frac{3}{2} Re\right)^{-1/2}\frac{\rho_\infty^2 R_1^2}{\mu_\infty}\frac{\rho}{\rho_\infty} Y_O Y_F A_R \exp(-E_R/RT) \tag{25}$$

Since the profiles of variables are axisymmetric, the stream function, temperature, and concentration profiles are further expanded with respect to the azimuthal angle σ as follows

$$\psi = \left(\frac{3}{2} Re\right)^{1/2} [\sigma F_0(\eta) + \sigma^3 F_1(\eta) + \ldots] \tag{26}$$

$$\frac{T - T_\infty}{T_\infty} = G_0(\eta) + \sigma^2 G_1(\eta) + \ldots \tag{27}$$

$$\frac{Y_O - Y_{O_\infty}}{Y_{O_\infty}} = H_0(\eta) + \sigma^2 H_1(\eta) + \ldots \tag{28}$$

$$\frac{Y_F}{Y_{O_\infty}} = I_0(\eta) + \sigma^2 I_1(\eta) + \ldots \tag{29}$$

The above expressions are substituted into Eqs. (22–25) and expanded in terms of the azimuthal angle σ. By comparing the coefficients of σ, a set of ordinary differential equations can be obtained. The boundary conditions are also transformed in a similar manner. All of the details of the derivations are reported in Ref. 6.

The governing equations of the gas and the solid phases are coupled and nonlinear. A value of surface temperature is first assumed to decouple the gas phase equations from the solid phase equation. The second-order nonlinear ordinary differential equations are transformed into initial value problems through the process of quasilinearization.[15] These equations can then be easily solved by using the Runge-Kutta method. Finally, the gas phase solutions and the solid phase solutions are matched on the fuel surface; that is, Eq. (11d) must be satisfied. The fuel properties and the related parameters adopted are shown in Table 1. Since the trigonometric terms are well-approximated by the leading two terms up to the azimuthal angle of 100 deg in Eqs. (26–29), the following discussion is based on the solution of the first leading two terms of the expansions.

The zero heat flux, $dq/dt = 0$, at the solid surface is chosen as the ignition criterion of the model.[6] Although the ignition criterion is adopted at the particle surface, it truly indicates the gas phase reaction in the boundary layer as well as its effect on the particle surface. When the PMMA particle is being heated in the hot convective flow, the temperature difference between the freestream and the PMMA particle surface becomes smaller as time goes on. As a result, the diffusive heat flux rate from the gas phase to the particle surface keeps decreasing. In the meantime, the chemical reaction rate of the gasified reactive vapor in the boundary layer is getting stronger, and so is the chemical heat released rate. At the time it overcomes the effect of thermal diffusion, the heat flux to the particle surface begins to increase with time, and then the temperature of the gas phase in the boundary layer runs up abruptly and ignition occurs. Therefore, the criterion adopted in this model should properly reveal the situation of gas phase ignition. Yang et al.[6] also showed that a strong temperature peak appeared in the boundary layer as the criterion of $dq/dt = 0$ is fulfilled.

Experiments

A schematic diagram illustrating the experimental apparatus is shown in Fig. 2. Air, heated by two 5-kW ceramic heaters, flows upward through several regulating screens and enters a 6-cm-diam, 30-cm-long Pyrex cylindrical test section to ignite the PMMA particle. The PMMA particle is suspended on a piece of 0.3-mm-diam stainless wire, which is attached to a 2-cm-diam stainless rod, and placed in the test section for ignition test.

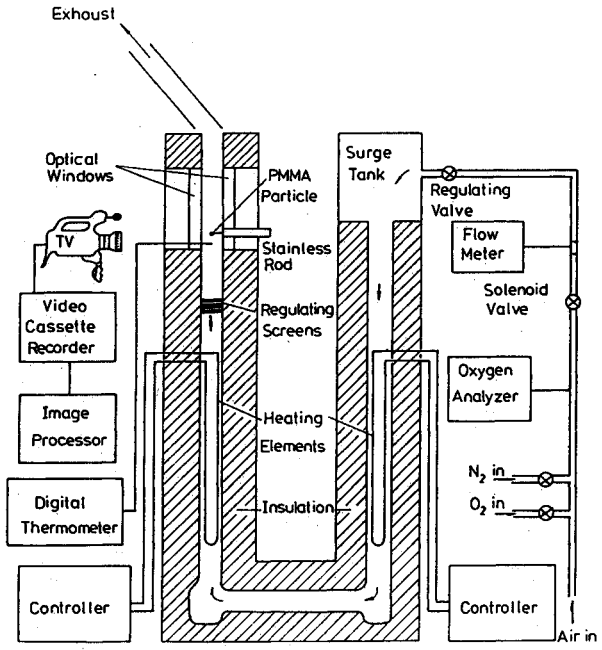

Fig. 2 Schematic diagram of the experimental apparatus.

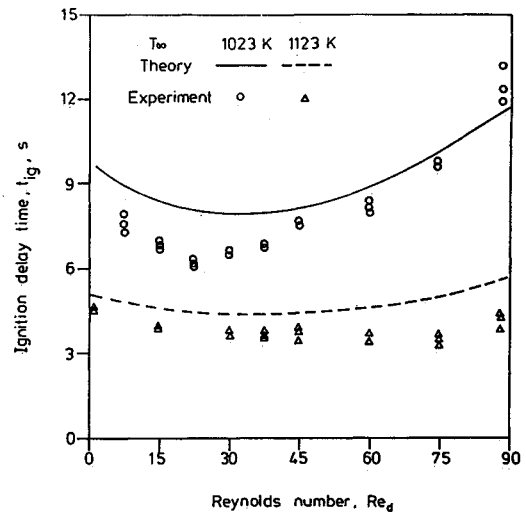

Fig. 3 Variation of the ignition delay time with Reynolds number for different gas temperatures (d = 10 mm, Y_{O_∞} = 0.23).

Table 1 PMMA properties and the related parameters adopted in the theoretical model[16–18]

PMMA	
ρ_s = 1.19 g/cm^3	A_R = 30,000,000 cm^3/g·s
α_s = 0.00082 cm^2/s	E_R = 7100 cal/mol
k_s = 0.0005 cal/cm·s·K	A_P = 100 cm/s
L = 380 cal/g	E_P = 12,800 cal/mol
Q = 6300 cal/g	T_i = 298.2 K
n = 6	
Radiation properties	
$\epsilon_w = 0.9$, $\epsilon_{wa} = 0.95$, $\epsilon_1 = \epsilon_2 = 1$	
$F_{w-wa} = 0.9764$, $T_{wa} = T_\infty - (520 - au_\infty)$, $a = 0.8$ K·s/cm	
$F_{w-1} = 0.0211$, $T_1 = T_\infty$	
$F_{w-2} = 0.0025$, $T_2 = 300$ K	
Gas phase	
$Pr = 0.7$	
C_P, k_∞, ρ_∞, μ_∞ properties of air at $T = T_\infty$	

The whole ignition process is recorded using a color video camera, with time resolution of 0.033 s. The ignition delay time is chosen as the time duration between the introduction of the particle into the hot air and the first appearance of flame around the particle surface. The properties of the PMMA specimen used in this experiment are shown in Table 1.

Results and Discussion

The comparisons of the ignition delay times between the experimental data and the theoretical results are shown in Figs. 3 and 4. Although it is very difficult to compare precisely the experimental results with the theoretical ignition criterion without the detailed transient temperature distribution, the ignition delay time observed in this experiment should be suitable for the verification of the model. The comparisons reveal that the model predictions agree reasonably well with the experimental results both qualitatively and quantitatively.

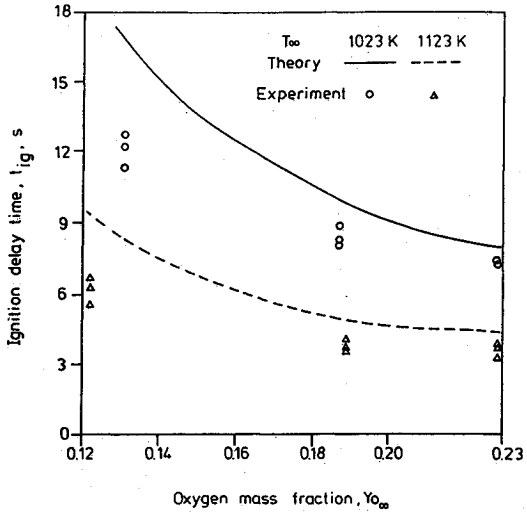

Fig. 4 Variation of the ignition delay time with oxygen mass fraction for different gas temperatures (d = 10 mm, Re_d = 45).

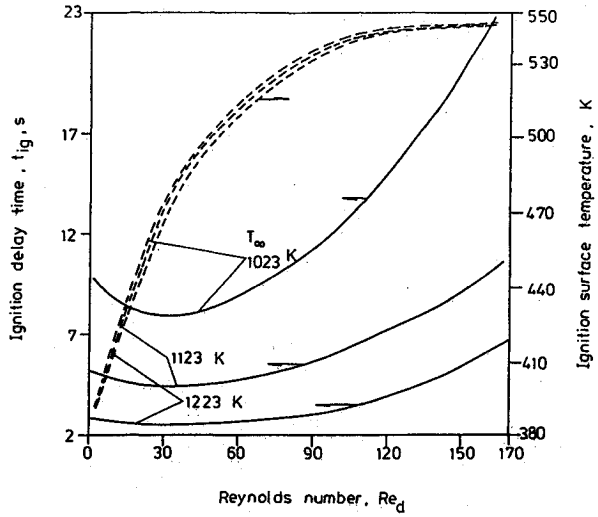

Fig. 5 Variation of the ignition delay time and ignition surface temperature with Reynolds number for different gas temperatures (Yo_∞ = 0.23, d = 10 mm).

Ignition Delay Time and Ignition Mechanism

The experimental data and the theoretical results in Fig. 3 show a similar trend. As the Reynolds number increases, the ignition delay time first decreases and then increases. This pattern agrees with the results of Refs. 6, 10, and 11 and is attributed to the shift of the dominant controlling mechanisms from pyrolysis to chemical kinetics as the Reynolds number increases.

The pyrolyzing rate of fuel increases as the Reynolds number increases due to higher heating rate. The stretch rate, which is equal to $3u_e \cos \sigma/2R_1$ in this study, increases with increasing Reynolds number or decreasing particle size and decreases with increasing azimuthal angle. The pyrolysis characteristic time is larger than the chemical reaction characteristic time at lower Reynolds nmbers; hence, the ignition process is pyrolysis-controlled, and the ignition delay time decreases with increasing Reynolds number. At higher Reynolds numbers, where the stretch rate is high, the dominant controlling mechanism is chemical kinetics, and the ignition delay time increases with increasing Reynolds number.

Figure 5 shows the theoretical ignition delay time as a function of the Reynolds number at three different gas temperatures. The ignition delay time for fuel particles at low temperature, e.g., 1023 K, is strongly affected by the Reynolds number since it is located in the chemical kinetics control regime for Reynolds numbers greater than 30.

Figure 6 shows the dependence of the ignition delay time on the oxygen mass fraction for different Reynolds numbers. Lowering the oxygen mass fraction decreases the chemical reaction rate and increases the ignition delay time. The ignition process for low oxygen mass fraction tends to be kinetics-controlled. The ignition delay time increases abruptly with Reynolds number for lower oxygen mass fraction as shown in Fig. 6.

The dependence of the ignition delay time on the Reynolds number for different initial particle sizes is shown in Fig. 7. The ignition delay time for large particles, e.g., 15 mm, decreases with increasing Reynolds number, hence, the ignition process for large particles is controlled by pyrolysis for Reynolds numbers less than 140. On the other hand, for smaller particles, e.g., 5 mm, the stretch rate is relatively higher than that of larger particles, and the ignition delay time increases as the Reynolds number increases. Hence, the ignition process for smaller particles is kinetics-controlled. There exists a transition particle size, e.g., 10 mm, and the ignition delay time decreases at first and then increases as the Reynolds number increases.

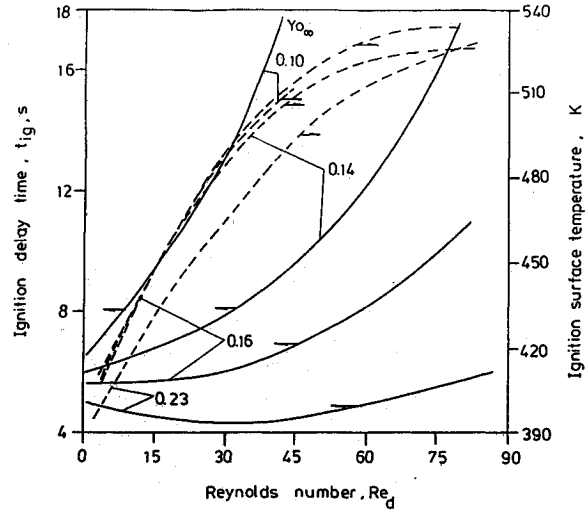

Fig. 6 Variation of the ignition delay time and ignition surface temperature with Reynolds number for different oxygen mass fractions (T_∞ = 1123 K, d = 10 mm).

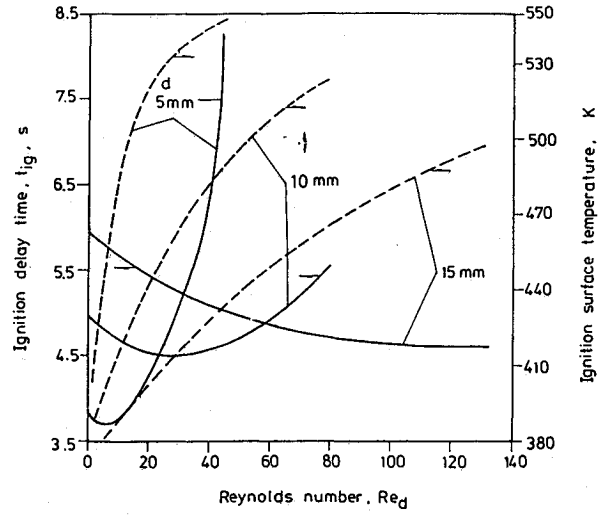

Fig. 7 Variation of the ignition delay time and ignition surface temperature with Reynolds number for different initial particle sizes (T_∞ = 1123 K, Yo_∞ = 0.23).

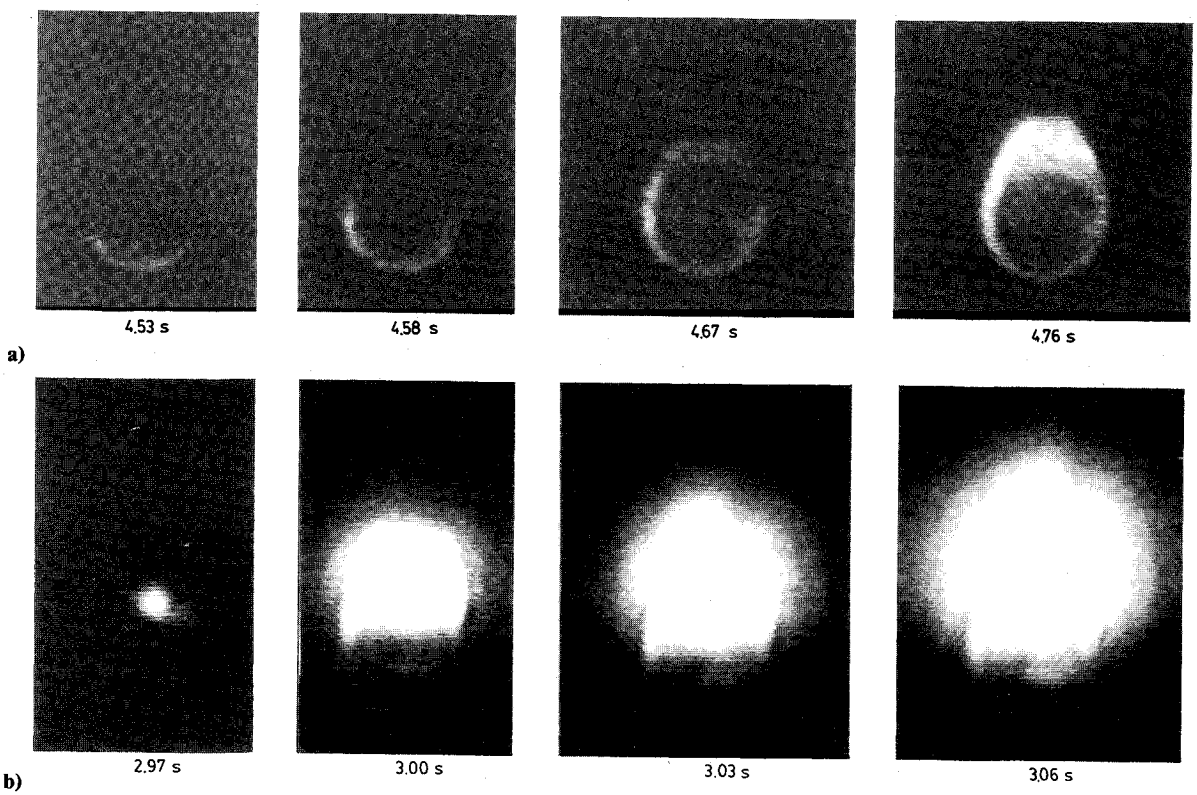

Fig. 8 Ignition process of a 10-mm PMMA particle under different controlling mechanisms: a) pyrolysis control, $T_\infty = 1123$ K, $Y_{O_\infty} = 0.23$, $Re_d = 0$; b) chemical kinetics control, $T_\infty = 1173$ K, $Y_{O_\infty} = 0.23$, $Re_d = 60$.

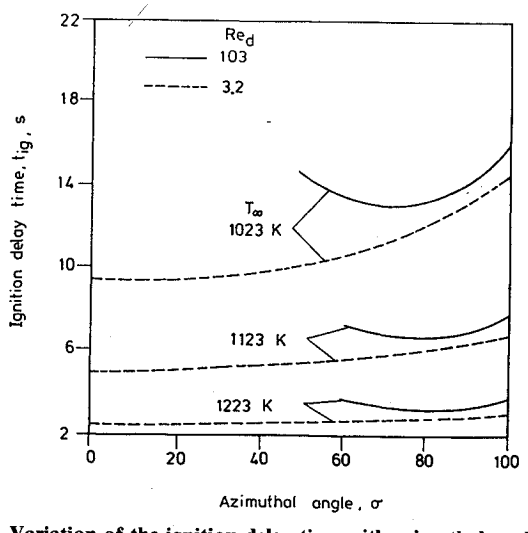

Fig. 9 Variation of the ignition delay time with azimuthal angle for different Reynolds numbers and gas temperatures ($d = 10$ mm, $Y_{O_\infty} = 0.23$).

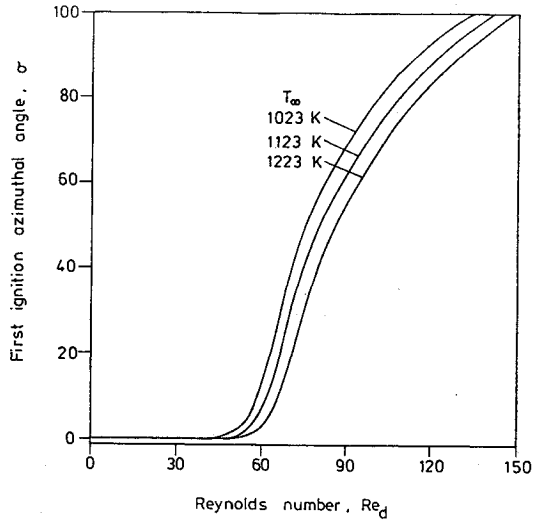

Fig. 10 Variation of the first ignition position with Reynolds number for different gas temperatures ($d = 10$ mm, $Y_{O_\infty} = 0.23$).

Ignition Surface Temperature

It can be seen from Fig. 5 that the surface temperature at ignition is insensitive to the gas temperature but is strongly affected by the Reynolds number. For higher Reynolds numbers, the pyrolyzed fuel vapor is much more easily swept away and, hence, needs a higher surface temperature, which implies a higher pyrolyzing rate, to achieve ignition. The dependence of the ignition surface temperature on the Reynolds number is much more profound than that on oxygen mass fraction, as depicted in Fig. 6.

The diffusion characteristic times for small particles is smaller than those of large particles, and so the pyrolyzed fuel vapor is more likely to be swept away before ignition. Hence, the ignition surface temperature for the small particles is higher than that of the large particles as shown in Fig. 7. It is therefore concluded that the ignition surface temperature is mainly affected by diffusion factors.

First Ignition Position

Many studies in the past on solid fuel ignition assumed that the first ignition occurred at the stagnation point.[10,11] In the present work, in addition to the stagnation point ignition, rearside ignition has been observed, as shown in Fig. 8. At low Reynolds numbers, the pyrolyzed vapor reacts with oxygen around the stagnation point region and ignition first occurs there. The flame then propagates downstream over the particle surface as shown in Fig. 8a. When the Reynolds number increases, the pyrolyzed vapor is swept downstream of the boundary layer and accumulates at the rearside of the particle. Ignition thus initiates there, and the flame propagates upstream as shown in Fig. 8b.

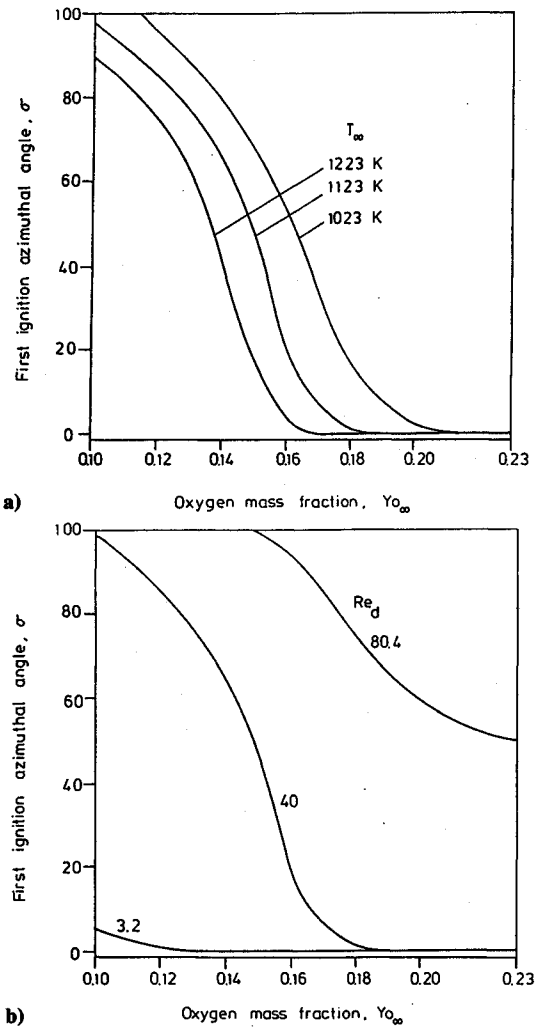

Fig. 11 Variation of the first ignition position with oxygen mass fraction: a) for different gas temperatures, $Re_d = 40$, $d = 10$ mm; b) for different Reynolds numbers, $T_\infty = 1123$ K, $d = 10$ mm.

On the theoretical aspect, this study predicts the same qualitative trend; the first ignition position shifted downstream at a higher Reynolds number as the experimental results. Figure 9 shows the ignition delay time as a function of azimuthal angle at different gas temperatures and Reynolds numbers. When the Reynolds number is low, the first ignition position is at the stagnation point, i.e., at an azimuthal angle of 0 deg. As the Reynolds number increases to 103, ignition position shifts downstream to an 80-deg azimuthal angle, judged by the minimum ignition delay time with respect to the azimuthal angle. This phenomenon is attributed to the assumption that the ignition may take place at the weaker stretch rate region, that is, at a larger azimuthal angle, where the chemical reaction is more active. The dependence of the first ignition azimuthal angle on the other parameters is determined in a similar way.

The effects of the Reynolds number and the gas temperature on the first ignition position are shown in Fig. 10. When the Reynolds number increases, the gasified fuel vapor is swept downstream and the ignition position shifts to larger azimuthal angles, where the reaction is more active. Varying gas temperature makes no distinct difference to the first ignition position.

Figure 11a illustrates the effect of oxygen mass fraction on the first ignition position at three different gas temperatures. Lowering the oxygen mass fraction reduces the reaction rate; hence the dominant ignition mechanism changes from pyrolysis to chemical kinetics. The first ignition position shifts downstream as oxygen mass fraction decreases. Figure 11b shows the dependence of first ignition position on the oxygen mass fraction at three different Reynolds numbers. Lowering oxygen mass fraction and increasing the Reynolds number make the first ignition position shift downstream.

Figures 12a and 12b demonstrate the effects of initial particle size, gas temperature, and Reynolds number on the first ignition position. The characteristic diffusion time for small particles is shorter. This makes the chemical kinetics the dominant controlling mechanism, and, therefore, the first ignition position shifts downstream for small size particles.

The first ignition position is determined by the competition between the chemical reaction rate and the diffusion rate, and the pyrolysis rate and the chemical reaction rate, respectively. If the diffusion rate is higher than the reaction rate, the ignition position shifts downstream. In general, increasing Reynolds number and decreasing initial particle size, gas temperature, and oxygen mass fraction make the first ignition position shift downstream.

In order to isolate the effects of the pyrolysis rate and the chemical reaction rate on the ignition position, the prefactors of the reaction rate and the pyrolysis rate are varied in this study. The results are shown in Fig. 13. When the pyrolyzing rate increases, the pyrolyzed fuel vapor cannot be consumed by chemical reactions immediately, and, hence, the ignition position shifts downstream. On the other hand, with an increase in chemical reaction rate, the pyrolyzed fuel vapor can be consumed rapidly, and, hence, the ignition position shifts upstream. In general, the role of pyrolysis is more influential on the first ignition position than that of the chemical kinetics.

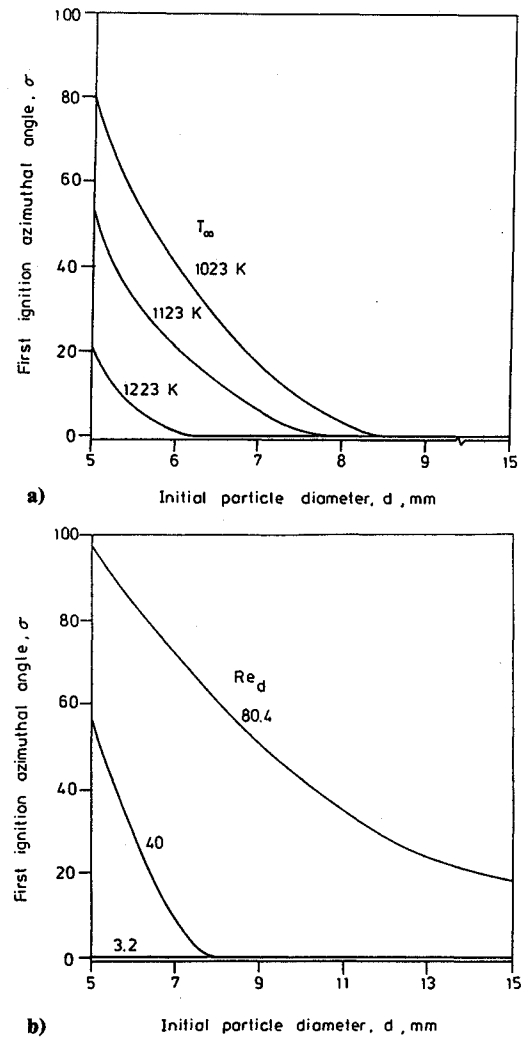

Fig. 12 Variation of the first ignition position with initial particle size: a) for different gas temperatures, $Re_d = 40$, $Yo_\infty = 0.23$; b) for different Reynolds numbers, $T_\infty = 1123$ K, $Yo_\infty = 0.23$.

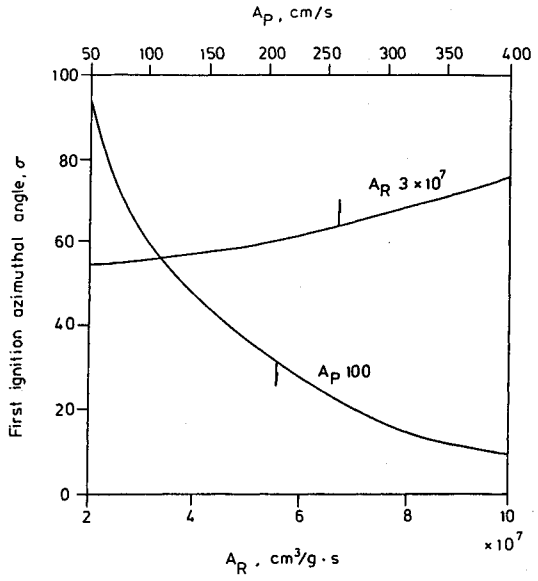

Fig. 13 Effect of changing pyrolyzing rate and chemical reaction rate on the first ignition position ($T_\infty = 1123$ K, $Re_d = 87$, $d = 10$ mm, $Y_{O_\infty} = 0.23$).

Conclusions

A theoretical model dealing with the ignition process of PMMA particles is developed. The validation of this model is verified by comparison with the experimental data. Some conclusions can be made as follows:

1) There exists a critical velocity for PMMA particle ignition in a convective environment. Below this velocity, the ignition controlling mechanism is pyrolysis, and the ignition delay time decreases as the Reynolds number increases. Above this velocity, the controlling mechanism is chemical kinetics, and the ignition delay time increases as the Reynolds number increases.

2) The ignition process for small size particles, low gas temperature, low oxygen mass fraction, and high Reynolds number tends to be controlled by chemical-kinetics. The ignition delay time at this regime is strongly affected by the Reynolds number and increases with the increasing Reynolds number.

3) Within the range of this study, the ignition process for large particles (15 mm) is controlled by pyrolysis and is controlled by chemical kinetics for small particles (5 mm).

4) The surface temperature at ignition is greatly affected by the Reynolds number and the initial particle size. Some minor influences come from the gas temperature and oxygen mass fraction.

5) The first ignition position is determined by the competitions among the diffusion rate, the pyrolysis rate, and the chemical reaction rate. The increasing diffusion rate and pyrolysis rate or the decreasing chemical reaction rate make the first ignition position shift downstream. In other words, the increasing Reynolds number and the decreasing gas temperature, oxygen mass fraction, and initial particle size make the first ignition point shift downstream over the fuel particle surface.

Acknowledgments

This work was financially supported by the National Science Council of the Republic of China, under Contract NSC 78-0401-E007-02. In addition, the authors would like to express their appreciation to S. C. Wang and Ai-Li Hsin Yang for their constructive discussions in editing.

References

[1]Deluca, L., Ohlemiller, T. J., Caveny, L. H., and Summerfield, M., "Radiative Ignition of Double Base Propellants: II. Pre-ignition Events and Source Effects," *AIAA Journal,* Vol. 14, No. 8, 1976, pp. 1111–1117.

[2]Kumar, R. K., "Gas Phase Ignition of a Composite Solid Propellant Subjected to Radiant Heating," *Combustion Science and Technology,* Vol. 30, 1983, pp. 273–288.

[3]Ohlemiller, T. J., and Summerfield, M., "Radiative Ignition of Polymeric Materials in Oxygen/Nitrogen Mixtures," *13th International Symposium on Combustion,* The Combustion Inst., Pittsburgh, PA, 1971, pp. 1087–1094.

[4]Fernandez-Pello, A. C., "An Analysis of the Forced Convective Burning of a Combustible Particle," *Combustion Science and Technology,* Vol. 28, 1982, pp. 305–313.

[5]Fernandez-Pello, A. C., and Law, C. K., "A Theory for the Free-Convective Burning of a Condensed Fuel Particle," *Combustion and Flame,* Vol. 44, 1982, pp. 97–112.

[6]Yang, J. T., Li, H. Y., and Wang, G. G., "On the Convective Thermal Ignition Process and Ignition Criteria of the Reactive Solid Particle," *Heat Transfer Phenomena in Radiation, Combustion, and Fires,* edited by R. K. Shah, American Society of Mechanical Engineers, New York, 1989, pp. 447–454.

[7]Niioka, T., "Heterogeneous Ignition of a Solid Fuel in a Hot Stagnation-Point Flow," *Combustion Science and Technology,* Vol. 18, 1978, pp. 207–215.

[8]Amos, B., and Fernandez-Pello, A. C., "Model of the Ignition and Flame Development on a Vaporizing Combustible Surface in a Stagnation Point Flow: Ignition by Vapor Fuel Radiation Absorption," *Combustion Science and Technology,* Vol. 62, 1988, pp. 331–343.

[9]Kim, C. S., and Chung, P. M., "Ignition of a Porous Solid Fuel by Convective Heat and Mass Transfer at the Fuel Surface," *Combustion Science and Technology,* Vol. 15, 1977, pp. 75–82.

[10]Niioka, T., Mitani, T., and Sato, J., "Ignition Characteristics of a Two-Component Condensed Fuel in a Stagnation-Point Flow," *20th International Symposium on Combustion,* The Combustion Inst., Pittsburgh, PA, 1984, pp. 1877–1882.

[11]Niioka, T., Takahashi, M., and Izumikawa, M., "Gas-Phase Ignition of a Solid Fuel in a Hot Stagnation-Point Flow," *18th International Symposium on Combustion,* The Combustion Inst., Pittsburgh, PA, 1981, pp. 741–747.

[12]Niioka, T., "Ignition Time in the Stretched-Flow Field," *18th International Symposium on Combustion,* The Combustion Inst., Pittsburgh, PA, 1981, pp. 1807–1813.

[13]Rangel, R. H., Fernandez-Pello, A. C., and Trevino, C., "Gas Phase Ignition of a Premixed Combustible by Catalytic and Non-Catalytic Cylindrical Surfaces," *Combustion Science and Technology,* Vol. 48, 1986, pp. 45–63.

[14]Kashiwagi, T., and Summerfield, M., "Ignition and Flame Spreading over a Solid Fuel: Non-Similar Theory for a Hot Oxidizing Boundary Layer," *14th International Symposium on Combustion,* The Combustion Inst., Pittsburgh, PA, 1973, pp. 1235–1247.

[15]Lee, E. S., *Quasilinearization and Invariant Imbeding,* Academic Press, New York, 1976, pp. 73–81.

[16]Kishore, K., Mohandas, K., and Annakutty, K. S., "Is Gasification Rate Controlling Step in Polymer Ignition?" *Combustion Science and Technology,* Vol. 31, 1983, pp. 183–194.

[17]Aseeva, R. M., and Zaikov, G. E., *Combustion of Polymer Material,* Hanser, New York, 1985, Chap. 2.

[18]Siegel, R. and Howell, J. R., *Thermal Radiation Heat Transfer,* 2nd ed., McGraw-Hill, New York, 1981, p. 830.